Journal of Molecular Liquids 344 (2021) 117727

Contents lists available at ScienceDirect

Journal of Molecular Liquids

journal homepage: www.elsevier.com/locate/molliq

Tuning the thermal properties of aqueous nanofluids by taking advantage of size-customized clusters of iron oxide nanoparticles

Amir Elsaidy [a], Javier P. Vallejo [b,*], Verónica Salgueiriño [a,c], Luis Lugo [a,c,*]

[a] CINBIO, Universidade de Vigo, 36310 Vigo, Spain
[b] Centro Universitario de la Defensa en la Escuela Naval Militar, Plaza de España, s/n, 36920 Marín, Spain
[c] Departamento de Física Aplicada, Universidade de Vigo, 36310 Vigo, Spain

ARTICLE INFO

Article history:
Received 14 June 2021
Revised 23 September 2021
Accepted 28 September 2021
Available online 5 October 2021

Keywords:
Fe_3O_4/γ-Fe_2O_3
Clusters
Solvothermal synthesis
Aqueous nanofluid
Cluster size
Iron oxide
Thermal conductivity

ABSTRACT

In this study, the thermal conductivity of aqueous nanofluids containing clusters of iron oxide (Fe_3O_4/γ-Fe_2O_3) nanoparticles has been investigated experimentally for the first time, with the aim of assessing the role of a controlled aggregation of nanoparticles in these final nanofluids. For that, clusters of iron oxide nanoparticles of different cluster size (46–240 nm diameter range) were synthesized by a solvothermal method and fully characterized by transmission electron microscopy, X-ray diffraction and Raman spectroscopy. The rheological behavior of the optimal nanofluids was also studied by rotational rheometry. The nanofluids were obtained by dispersing the clusters of iron oxide nanoparticles in water taking into account different solid volume fractions (from 0.50 to 1.5 wt%) and the experiments were conducted in the temperature range from 293.15 K to 313.15 K. The study reveals and quantifies enhancements in the thermal conductivity of nanofluid with increase of cluster size and temperature. Furthermore, a 0.50 wt% concentration of clusters of iron oxide nanoparticles within the whole range of proposed nanofluids offers great stability and improved thermal conductivity for heat transfer applications with an small dynamic viscosity increase. In addition, the larger the size of the clusters of iron oxide nanoparticles, the greater the increase in thermal conductivity for the designed Fe_3O_4/γ-Fe_2O_3 cluster-based nanofluids, with thermal conductivity values following a constant upward trend and reaching a maximum increase of 4.4% for the largest synthesized clusters (average size of 240 nm). These results open the door for the development of iron oxide-based nanofluids on which taking advantage of an optimized aggregation of nanoparticles by using size-customized clusters.

1. Introduction

The increasing demand of energy across the world has become a critical issue in our nowadays society. Limited fossil fuel, and its side effects largely contributing to air pollution, has forced the searching of alternative clean sources and the reduction in consumption of this fossil fuel through increasing efficiency of existing energy systems [1]. For instance, decreasing energy consumption based on enhancing fluids heat transfer efficiency has become a huge challenge, taking into account the main objectives of engineering and industry [2,3]. This objective should address for example the performance of the heat exchangers, that can be considerably enhanced by improving the thermal conductivity of working fluids [4–7].

Nanofluids, colloidal suspensions of nanoparticles or nanostructures in liquid carrier fluids as water, ethylene glycol and engine oil, contribute to exhibit a large thermal conductivity (TC) [8], of which the next generation heat transfer fluids can benefit, when applied in microelectronics, or for energy supply [6,9–11]. Indeed, a TC enhancement upon the dispersion of nanoparticles into a base fluid has been previously studied for heat transfer [8,12–15], and there are many different examples reporting improvements in the values of TC when using metallic (Fe, Cu) or metal oxide (Fe_3O_4) nanoparticles, at different concentrations, at different temperatures, using different average sizes and even taking into account the influence of an external magnetic field [2,11,16]. In this regard, different authors reported non-dependence in the enhancement ratios of this property with the increasing temperature. As an example, in the case of Fe_3O_4 nanofluids, the works by Parekh and Lee [17], Yu *et al.* [18] or Fu *et al.* [3] should be mentioned. On the contrary, some authors showed strong dependences of the thermal conductivity enhancement ratio with the increasing

* Corresponding authors.
E-mail addresses: jvallejo@cud.uvigo.es (J.P. Vallejo), luis.lugo@uvigo.es (L. Lugo).

https://doi.org/10.1016/j.molliq.2021.117727
0167-7322/

temperature for Fe_3O_4 nanofluids [1,8,9,11,19]. In the latter cases, the trends are especially prominent for high nanoparticle concentrations and high temperatures, where agglomeration or aggregates may have influenced the final results.

On this topic, it is particularly important to take into account that the particles stability in the suspension is key and accordingly, considerable research has been conducted in this regard [20,21]. However, given the fact that there is no control in the likely aggregation of the nanoparticles above a threshold concentration when dispersed in these fluids designed to work in heat exchangers, the effects a controlled aggregation can exert in the nanofluids thermal properties have not been studied so far. Appropriately, herein we report for the first time the use of a spherical assembly of iron oxide nanoparticles of controlled size, i.e. Cluster of Iron Oxide Nanoparticles (CION), such that we can study the influence of this controlled aggregation in the final effective TC and be able to propose tuned nanofluids using these particular nanostructures. For that, we have synthesized CION with tailored average sizes (from 46 to 240 nm) using a solvothermal method, and have fully characterized them by transmission electron microscopy, X-ray diffraction and Raman spectroscopy. The chosen clusters were dispersed in water to obtain aqueous nanofluids using different concentrations, of which the thermal conductivities and dynamic viscosities were obtained through the herein detailed careful analysis.

2. Experimental section

2.1. Chemicals

Iron(III) chloride hexahydrate ($FeCl_3{\cdot}6H_2O$ (>99%), sodium acetate (>99%), poly(ethylene glycol) (MW 6000, PEG6000), ethylene glycol (>99%) were purchased from Sigma-Aldrich and Water (Milli-Q). All chemicals were used as received.

2.2. Synthesis of clusters of Fe_3O_4/γ-Fe_2O_3 nanoparticles

The synthesis of clusters of iron oxide (Fe_3O_4/γ-Fe_2O_3) nanoparticles tuning the final size of the clusters was conducted through a synthetic procedure published elsewhere [22]. For the five types of clusters under consideration; 2.5 mmol (0.678 g) of $FeCl_3{\cdot}6H_2O$ were dissolved in 20 mL of ethylene glycol, and mechanically stirred up to form a clear solution, followed by the addition of sodium acetate (1.8 g) and PEG, in five independent experiments. For tuning the final size of the clusters, the amount of PEG employed was 12.5 wt%, 8.5 wt%, 2.5 wt%, 8 wt%, and 2.5 wt%, such that 46 nm (cluster **A**), 70 nm (cluster **B**), 111 nm (cluster **C**), 178 nm (cluster **D**), and 240 nm (cluster **E**) average diameter clusters were obtained, respectively. In all cases, the mixture was first homogenized, and then sealed in a stainless steel autoclave (100 mL). The autoclave was heated up to 458.15 K (heating rate: 5 K/min) while mechanically stirring (1500 rpm for clusters **A**, **B** and **C** and 800 rpm for clusters **D** and **E**) the solution for 8 h. Finally, the mixture was allowed to cool down to room temperature and the black product was collected using a magnet. The clusters were then washed several times with Milli-Q water and dried overnight at 333.15 K in an oven, such that five different clusters of magnetic nanoparticles were available.

2.3. Preparation of aqueous nanofluids using clusters of Fe_3O_4/γ-Fe_2O_3 nanoparticles

Different nanofluids were prepared dispersing clusters **A**, **B**, **C**, **D** and **E** in Milli-Q water, using a 0.50 wt% mass fraction in all the cases (0.50 wt% nanofluid **A**, 0.50 wt% nanofluid **B**, 0.50 wt% nanofluid **C**, 0.50 wt% nanofluid **D**, and 0.50 wt% nanofluid **E**). Furthermore, nanofluids using a 0.10 wt% mass fraction of clusters **A** and **D** (0.10 wt% nanofluid **A** and 0.10 wt% nanofluid **D**) and additional mass fractions of clusters **E** (1.0 and 1.5 wt%) were also considered (1.0 wt% nanofluid **E**, and 1.5 wt% nanofluid **E**).

2.4. Characterization

Transmission electron microscopy (TEM) measurements were performed on a JEOL JEM 1010 instrument (JEOL, Tokyo, Japan) operating at an acceleration voltage of 100 kV. Samples for the TEM analysis were prepared by dropping a diluted suspension of the clusters onto an ultrathin carbon-coated copper grid. X-ray diffraction (XRD) patterns were collected by using a Siemens D-5000 powder X-ray diffractometer ($Cu_{K\alpha}$ radiation (λ = 1.54056 Å) in the range 2θ = 5–100°) and compared with the crystallographic information files (CIF) from the crystallographic open data base (COD). Raman spectra were collected in powder samples onto a glass slide as substrate, with a Renishaw in Via Reflex Raman Microscope (Renishaw, Gloucestershire, UK). Experiments were conducted at room temperature by using an excitation wavelength of 633 nm.

The stability of the dispersions was evaluated by zeta potential and dynamic light scattering analyses using a Zetasizer Nano ZS (Malvern Instruments Ltd, Malvern, United Kingdom). The zeta potential was determined for 0.10 wt% CION-based aqueous nanofluids with cluster sizes of 46 and 178 nm (clusters **A** and **D**, respectively) at different temperatures in the range from 283.15 K to 323.15 K. The apparent sizes of the nanoadditives within these same dispersions were determined for 30 days at 298.15 K, using a dispersion angle of 173°. For each different-sized dispersion, two samples were analyzed under different conditions. One of them remained in static conditions from preparation throughout the measurement period (hereinafter, static dispersion). The other sample was mechanically shaken for 1 min at 2000 rpm prior to the dynamic light scattering (DLS) measurement (hereinafter, shaken dispersion) using a ZX3 Advanced Vortex Mixer (VELP Scientifica SRL, UsmateVelate, Italy).

The thermal conductivity (TC) of nanofluids and base fluid was experimentally determined in the temperature range from 293.15 K to 313.15 K by a THW-L2 thermal conductivity-meter (Thermtest Inc., New Brunswick, Canada) coupled with an EchoTherm IC20XR dry bath that allows the temperature control using Peltier technology. The operation of this device is based on the transient short-hot-wire (SHW) technique, in accordance with the ASTM D7896-14 standard [23]. The aluminum wire is 60 mm long and 0.1 mm in diameter. It is inserted vertically into the container with 18 mL of sample inside. The whole assembly is placed on the dry bath, covered with an insulating case, and the necessary time is waited to achieve the desired temperature. An initial power test serves to adjust the heating power required to produce the local temperature rise necessary for the measurement in a short period of time (~2 s), avoiding natural convection phenomena. The adequacy and precision of this device for nanofluids has been previously validated elsewhere [24–26]. Five tests were made per sample and temperature, in order to ensure the repeatability of the values, waiting 3 min between measurements. The expanded uncertainty of the values obtained through this device is declared as 2%.

The rheological behavior of nanofluids and base fluid was studied at 293.15 K by a Physica MCR 101 rotational rheometer (Anton Paar, Graz, Austria) coupled with a CP50-1 cone-plate geometry (diameter = 50 mm, cone angle = 1°, cone truncation = 102 μm). The temperature of the sample was stablished by a P-PTD 200 Peltier system, waiting a stabilization period of at least 100 s before operating. The test procedure consisted of obtaining the flow

curves of the samples in the shear rate range from 1 to 1000 s^{-1} with 10 point per decade. The expanded uncertainty of the dynamic viscosity measurements is 3%.

3. Results and discussion

The clusters of iron oxide (Fe_3O_4/γ-Fe_2O_3) nanoparticles herein studied were obtained through a solvothermal method, by which the mechanism of formation proceeds via a two-stage growth process, with nucleation of primary nanocrystals followed by uniform and controlled aggregation into larger secondary nanostructures [27]. This process to obtain CION with tuned size (the final size of the clusters and of the nanoparticles forming them) depends mainly on the poly (ethylene glycol) (PEG) concentration in the reaction medium [22]. Fig. 1 includes the TEM and the size distribution analysis (Gaussian fit) of the five different types of clusters under consideration, from now on (color-coded) clusters **A**, **B**, **C**, **D**, and **E** with average diameters of 46 ± 14 nm, 70 ± 19 nm, 111 ± 21 nm, 178 ± 21 nm, and 240 ± 37 nm, respectively.

Fig. 2 includes the structural characterization of the five types of clusters, taking into account X-ray diffraction (XRD) and Raman spectroscopy. The XRD analysis of these clusters shows five similar patterns (Fig. 2a), on which we observe well-defined peaks that correspond to a spinel structure, though with different noise attending to the different size of the crystalline domains forming part of the nanoparticles in the final clusters [27]. Since the XRD data of spinels (i.e. maghemite, magnetite or other transition metal ferrites) show very similar diffraction patterns because all of them

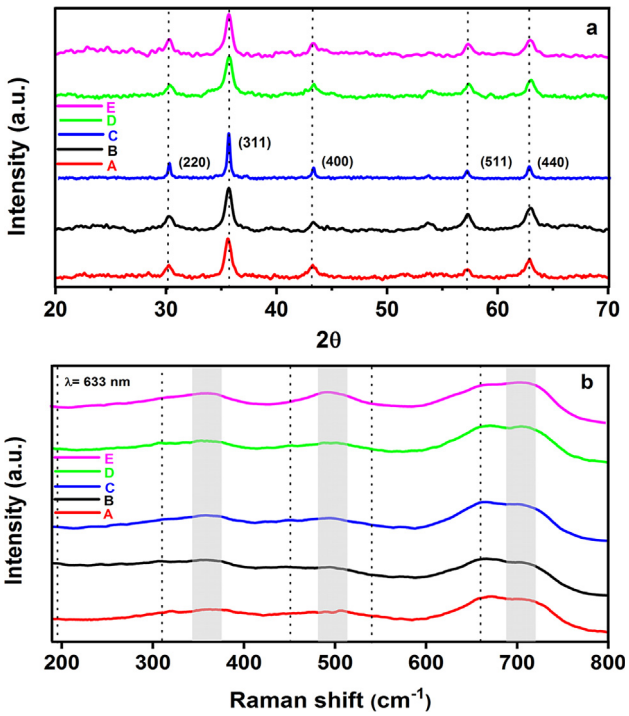

Fig. 2. XRD patterns (a) and Raman spectra registered using a 633 nm excitation wavelength (b) of clusters **A**, **B**, **C**, **D**, and **E**.

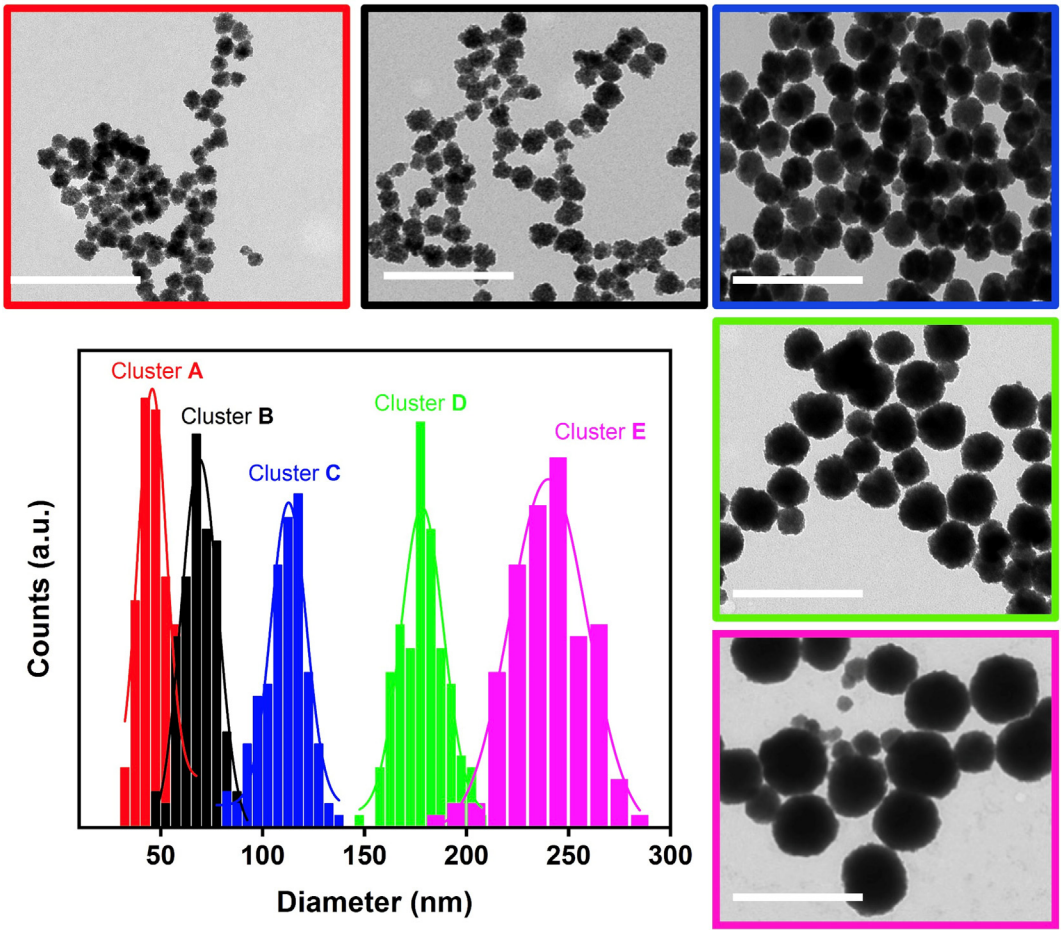

Fig. 1. TEM images (clockwise, scale bar: 500 nm, magnification 10,000x) and particle size distribution analysis of clusters **A** (framed in red), **B** (black), **C** (blue), **D** (green), and **E** (magenta).

share the same crystalline structure, we have further characterized the powders of clusters using Raman spectroscopy. This technique is a powerful means to investigate structural properties of materials, and can provide unique information when analyzing nanostructured transition metal oxides [28], as registering the different vibrations due to different cationic arrangements [29]. In the particular case under study, with a magnetic iron oxide phase prone to oxidation, we have used an excitation wavelength of 633 nm to achieve a satisfactory penetration depth while avoiding any further oxidation of the clusters. Attending to the Raman spectra obtained for the samples, we have included in the graph in Fig. 2b the expected group theory vibration modes of both magnetite (Fe_3O_4, vertical dotted lines) and maghemite (γ-Fe_2O_3, shaded grey areas) iron oxides phases. That is, five main bands appearing at 196, 306, 460, 538 and 668 cm^{-1}, corresponding to the T_{2g} (1), E_g, T_{2g} (2),T_{2g} (3),and A_{1g} modes of magnetite, respectively, and three broad bands centered at 350, 500 and 700 cm^{-1}, corresponding to the T_{2g}, E_g and A_{1g} modes of maghemite, respectively [30,31]. According to this, the Raman spectra confirm the presence of both oxides in the five types of clusters, considering the very intense A_{1g} band of magnetite and the three main bands of the maghemite (present in all the cases), though likely with a different ratio of iron oxide phases. In this regard, other characteristic features of the materials like the black coloration of its powders and their strong interaction with external magnetic fields were also observed.

Fig. 3a shows the quasi-constant zeta potential values obtained for the dispersions of different-sized CION at the analysed temperatures. This trend implies that there are no remarkable differences in the intensity of the electrostatic repulsion forces among the nanoadditives in the temperature range analysed. Therefore, similar conditions can be inferred in relation to the stability of the dispersions. Generally, absolute zeta potential values>30 mV are considered a symptom of stability of nanofluids in the literature [32–34]. Furthermore, it is also implied that the higher this value, the greater the dispersion stability, due to higher electrostatic repulsion forces between clusters, which avoid coalescence between them and subsequent sedimentation. The average zeta potential values are 39.1 and 30.1 mV for the clusters with average diameters of 46 nm (0.10 wt% nanofluid **A**) and 178 nm (0.10 wt% nanofluid **D**), respectively. Both values exceed the threshold of 30 mV, considered a sign of moderate stability. A relationship can be observed between the increase in the size of the clusters and the decrease in the value of the zeta potential. The nanofluid based on smaller clusters has a higher zeta potential value, indicating potentially better performance in terms of stability.

Fig. 3b and 3c show the evolution of the Z-average size (or hydrodynamic size) with the time since preparation. Z-average size is the intensity-weighted mean size calculated from a cumulants fit autocorrelation function of intensity. It should be noted that DLS measurements assume that the measured nanostructures are perfect spheres offering an average diameter, taking into account the hydrodynamic size, that is, the real size plus the three-dimensional extension of the electrostatic double layer that renders them stable in dispersion. Therefore, the measurement of this apparent size correlates with the colloidal stability of the nanostructures under study, focusing therefore the analysis on this stability evolution.

Fig. 3b evidences that similar size values were obtained for 0.10 wt% nanofluid **A** during the 30 days of analysis, both for static and shaken dispersions. This confirms the very good stability of this nanofluid already pointed out by the zeta potential results plotted in Fig. 3a. Fig. 3c shows that while the static dispersion of 0.10 wt% nanofluid **D** undergoes a partial sedimentation overtime, the shaken dispersions keep a similar size value over the analyzed period. This implies that though the clusters within the

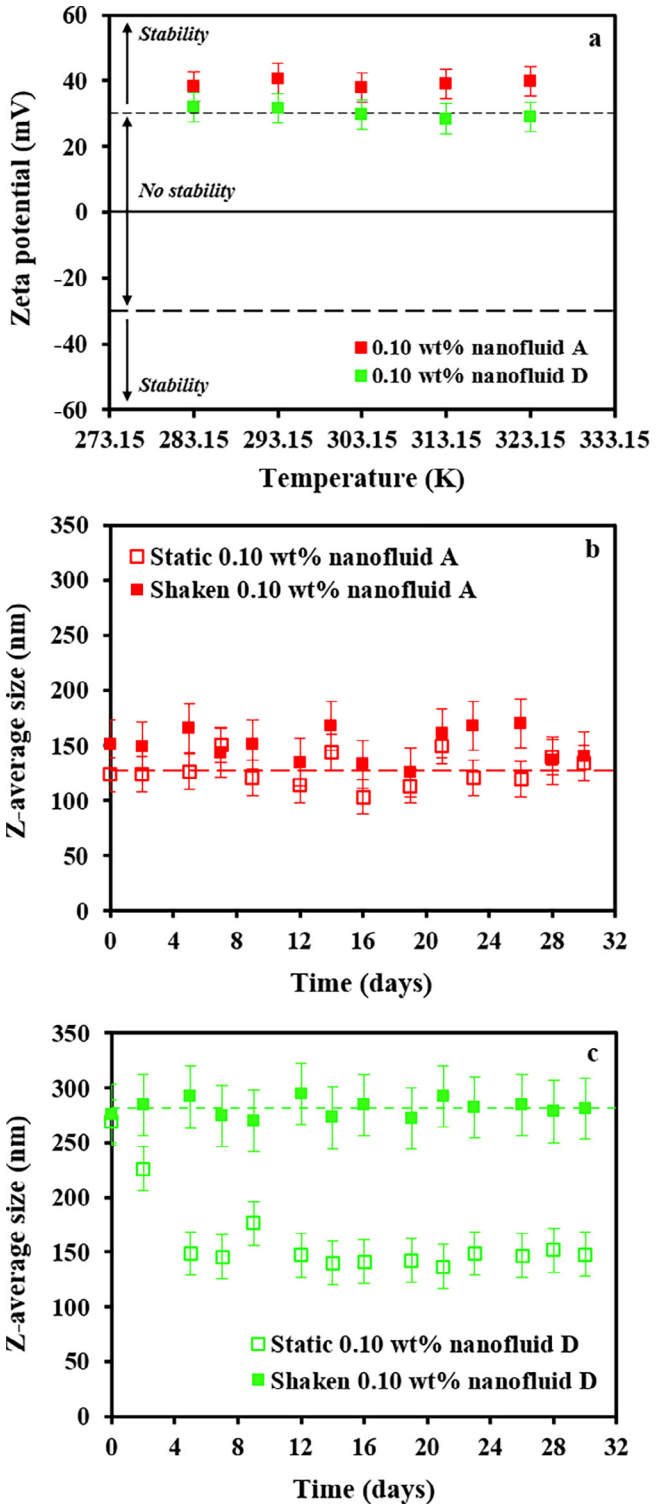

Fig. 3. Zeta potential as a function of temperature (a) and average Z-Size as a function of time after preparation (b and c) for 0.10 wt% nanofluids **A** and **D**. Error bars mean standard deviation for each measurement.

nanofluid tend to clump together and sediment with time, a simple mechanical agitation achieves the initial dispersibility conditions as counteracting the moderate coalescence process and enabling their potential use in practical applications.

The nanofluids were prepared by dispersing the CION powder in water taking into account different solid mass fractions (from 0.50 to 1.5 wt%), from which the experimental thermal conductivities

(TC) data were measured. For the set of analyzed nanofluids, Table 1 and Table 2 allow us to analyze the influence of the cluster size, temperature and nanoadditive (that is, CION) concentration on the detected variations.

Fig. 4 and Table 1 evidence that, the larger the cluster size, the greater the TC increase for the designed CION-based nanofluids. The values obtained follow a constant upward trend, reaching a maximum increase of 4.4% for the largest synthesized nanostructures (CION with an average diameter of 240 nm), as shown in Fig. 4. Our novel results for these CION-based nanofluids confirm the generic relation between nanoparticle/nanostructure size and nanofluid TC, previously established for other nanofluids constituted by other types of nanoadditives.

Beck *et al.*[35] analysed different-sized (8–282 nm) alumina dispersions in water and ethylene glycol, obtaining the higher TC values for the largest nanoparticles and clearly lower TC increments for particle sizes below 50 nm. They associate this minor improvement with a decrease in the thermal conductivity of the metal oxide nanoparticles themselves, given their sufficiently small size promoting greater phonon scattering, assuming different rates of phonon transport at the solid-liquid interfaces [35]. Sobczak *et al.* [26] analysed different-sized (13 and 30 nm) carbon black dispersions in ethylene glycol, confirming the higher TC for the largest nanoparticles. They attributed these results to the relationship between larger size and larger specific surface area, generally related to larger TC increases.

Lately, the aggregation of nanometric particles and/or the existence of a nanolayer (of liquid molecules likely behaving differently because interacting with the atoms/charges at the surface of the nanoparticles) at the solid-liquid interface are recognized as the main reasons that explain the TC increase for nanofluids in literature [36–38]. In this regard, liquid molecules near the surfaces of nanoparticles were hypothesized to allow the creation of layered structures that tend to exhibit solid-like behaviour [37], and have a notable influence on the improvement of the nanofluid TC [38]. Another issue is related to the fact that nanoadditives with larger sizes can produce reductions in the contact resistance that leads to superior TC [26].

Fig. 5 shows practically the same TC increases for each nanofluid with different-sized clusters at the three analysed temperatures. This non-dependence of the TC enhancement ratios with the increasing temperature agrees with the established knowledge in the literature [39,40] and with long term stability of the proposed dispersions. Moreover, as pointed, different authors presented this same behaviour for Fe_3O_4 nanofluids: Parekh and Lee [17] for water based nanofluids in the temperature range from 25 to 65 °C, Yu *et al.* [18] for kerosene based nanofluids in the temperature range from 10 to 60 °C, or Fu *et al.* [3] for ethylene glycol-water based nanofluids in the temperature range from 30 to 60 °C. Moreover, similar results were also reported for other types of water based nanofluids [41–43]. On the contrary, some authors showed strong dependences of the TC enhancement ratio with the increasing temperature for Fe_3O_4 nanofluids [1,8,9,11,19]. Nevertheless, it should be noted that the trends reported there are especially prominent for high nanoparticle concentrations and high temperatures, where agglomeration or aggregates may have influenced the final results.

Maxwell, Bruggeman or Hamilton-Crosser postulated some of the classical models to determine the thermal conductivity of solid-liquid mixtures with micro-sized (or even higher) particles

Table 2
Thermal conductivity of CION-based aqueous nanofluids (clusters **E**, 240 nm) for different nanoadditive concentrations at 293.15 K.

Nanofluid	Thermal conductivity ($W \cdot m^{-1} \cdot K^{-1}$)
0.50 wt% nanofluid **E**	0.626
1.0 wt% nanofluid **E**	0.619
1.5 wt% nanofluid **E**	0.618

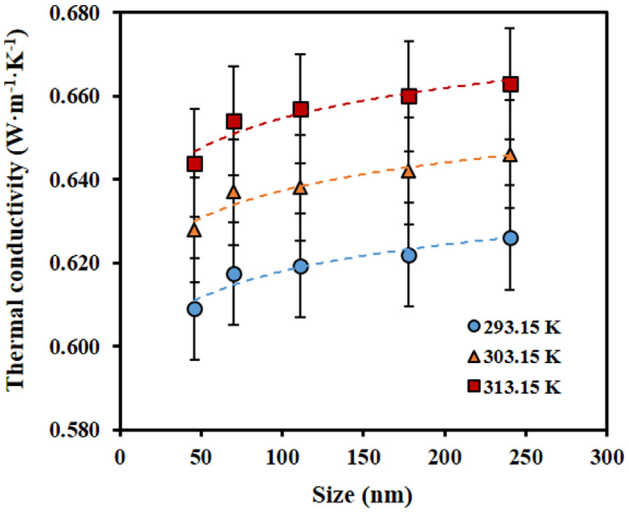

Fig. 4. Thermal conductivity of 0.50 wt% CION-based aqueous nanofluids as a function of cluster size at different temperatures. Error bars mean expanded uncertainty.

Table 1
Thermal conductivity of 0.50 wt% CION-based aqueous nanofluids for different cluster sizes and temperatures.

Nanofluid	CION size[1] (nm)	Z-average size[2] (nm)	Temperature (K)	Thermal conductivity ($W \cdot m^{-1} \cdot K^{-1}$)
0.50 wt% nanofluid **A**	46 ± 14	124 ± 16	293.15	0.609
			303.15	0.628
			313.15	0.644
0.50 wt% nanofluid **B**	70 ± 19	149 ± 15	293.15	0.617
			303.15	0.637
			313.15	0.654
0.50 wt% nanofluid **C**	111 ± 21	192 ± 16	293.15	0.619
			303.15	0.638
			313.15	0.657
0.50 wt% nanofluid **D**	178 ± 21	270 ± 20	293.15	0.622
			303.15	0.642
			313.15	0.660
0.50 wt% nanofluid **E**	240 ± 37	356 ± 23	293.15	0.626
			303.15	0.646
			313.15	0.663

[1] Data from TEM analysis of the clusters.
[2] Data from dynamic light scattering analysis of the nanofluids just after preparation.

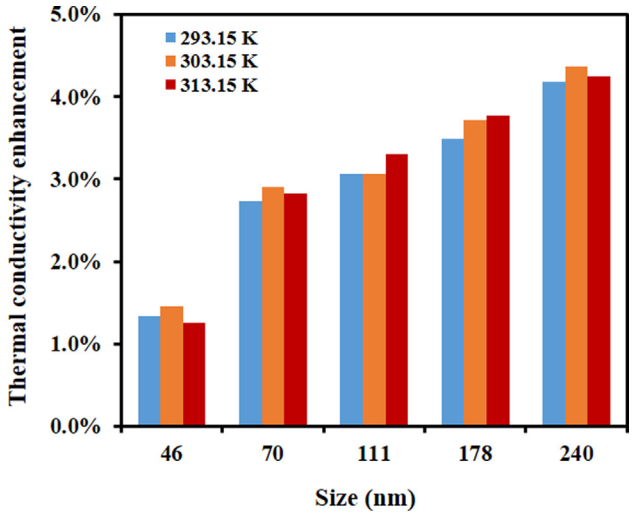

Fig. 5. Thermal conductivity enhancements of 0.50 wt% CION-based aqueous nanofluids as a function of cluster size at different temperatures.

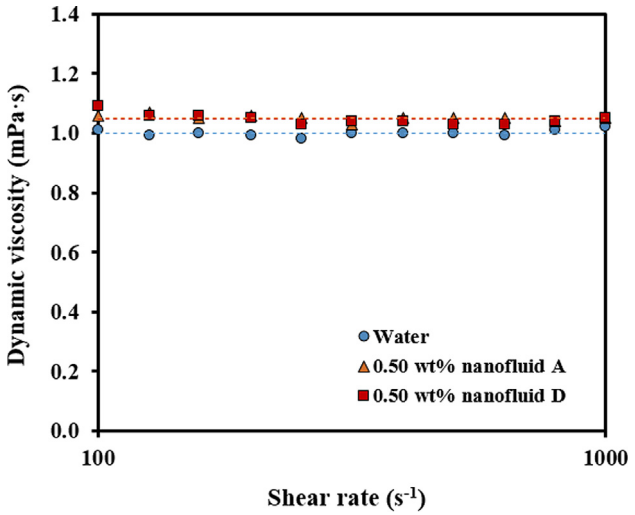

Fig. 6. Flow curves for water and 0.50 wt% nanofluids **A** and **D** in the shear rate range from 100 to 1000 s^{-1} at 293.15 K.

[44]. These models suggest that the thermal conductivity of the mixture is mainly based on the thermal conductivity of the solid and the fluid and the particle volume fraction. Likewise, these models have been also widely tested in the field of nanofluids and is well recognized that all give similar results for spherical nanoparticles and low concentrations [44]. Thermal conductivities of 3.5–7.0·m^{-1}·K^{-1} and 0.9–1.3 W·m^{-1}·K^{-1} are reported for magnetite [45–47] and maghemite [48], respectively. The 0.005 mass fraction of CION corresponds to a 0.001 vol fraction by using a density value of 5.0 g·cm^{-3}. Taking into account the previous data, deviations between experimental and calculated data of 1.0–1.3%, 2.5–2.9%, 2.8–3.3%, 3.3–3.7%, and 3.9–4.3% were obtained for the 0.50 wt% aqueous nanofluids with CION sizes of 46, 70, 111, 178, and 240 nm, respectively. As observed, the classical models present the best results for the lower-sized clusters. Nevertheless, it should be noted that these models do not consider particle size (an important variable, as we report here) as well as many other phenomena generally reported as contributors to the increased thermal conductivity of nanofluids (layering between liquid and solid nanoparticles, clustering, Brownian motion, micro-convection, thermophoretic effect, etc.) [49].

Table 2 reveals that an increase on the CION concentration above 0.50 wt% has no significant influence on the modification of thermal conductivity. According to the literature, the value of thermal conductivity tends to increase with increasing concentration of nanoadditive, as has been pointed out in multiple experimental works [50] and is predicted by most of the theoretical models [51]. However, this trend is related by some authors [50,52–54] with a limited nanoparticle loading above which the increase in thermal conductivity stops. In this regard, increasing the concentration also often causes the viscosity to increase, so the pumping power required to make the fluid flow will also be higher, which implies a deleterious effect. Therefore, 0.50 wt% solid mass concentration in the final nanofluid becomes more convenient in the final applications, given the greater stability and thermal conductivity associated and the lower pumping power consumption required.

The rheological behavior of the 0.50 wt% nanofluids and base fluid was assessed by analyzing their flow curves at 293.15 K. Fig. 6 shows the obtained viscosity values in the 100–1000 s^{-1} shear rate range for water and two 0.5 wt% nanofluids (45 and 178 nm cluster sizes), as an example. As observed, all samples show a Newtonian behavior in the analyzed shear rate range. The 0.50 wt% nanofluids showed a small dynamic viscosity increase of around 5% with respect to water. No significant differences are observed in the viscosity increase of the nanofluids with respect to the cluster size.

4. Conclusion

Clusters of iron oxide (Fe_3O_4/γ-Fe_2O_3) nanoparticles with average diameters ranging from 46 to 240 nm were synthesized and used to design aqueous nanofluids as heat transfer fluids. The thermal conductivity of these nanofluids in the temperature range from 293.15 K to 313.15 K are measured using a thermal conductivity-meter based on the transient short-hot-wire (SHW) technique. The study quantifies the thermal conductivity increases with increase of particle size and temperature for nanofluids with optimized cluster mass concentration of 0.50 wt%. The larger the cluster size, the greater the TC increase for the designed iron oxide cluster nanofluids. The values obtained follow a constant upward trend, reaching a maximum increase of 4.4% for the largest synthesized nanostructures (average size of 240 nm). Newtonian behavior with dynamic viscosity increases of around 5% with respect to water were found for the 0.50 wt% nanofluids with different-sized clusters. The results show that the 0.50 wt% mass fraction offers moderate long-term stability, the higher TC increase, and a low pumping power consumption increment with respect to water (in accordance with the slight dynamic viscosity increase). This study sheds light on conducting new clusters of nanoparticles to customized nanofluids with potential use in heat transfer applications.

CRediT authorship contribution statement

Amir Elsaidy: Investigation, Formal analysis, Data curation, Writing – original draft. **Javier P. Vallejo:** Conceptualization, Investigation, Formal analysis, Data curation, Writing – original draft. **Verónica Salgueiriño:** Conceptualization, Validation, Formal analysis, Writing – review & editing. **Luis Lugo:** Conceptualization, Validation, Formal analysis, Writing – review & editing.

Declaration of Competing Interest

The authors declare that they have no known competing financial interests or personal relationships that could have appeared to influence the work reported in this paper.

Acknowledgements

This work was supported by the "Ministerio de Economía y Competitividad" (Spain) and the FEDER program through the ENE2017-86425-C2-1-R and CTM2017-84050-R projects and by the "Ministerio de Ciencia e Innovación" (Spain) through the PID2020-112846RB-C21, PID2020-119242RB-I00 and PDC2021-121225-C21 projects. This work was also partially supported by the EU COST Action CA15119: Overcoming Barriers to Nanofluids Market Uptake, Nanouptake, and the EU COST Innovators Grant CIG15119: Nanofluids for Convective Heat Transfer Devices, NANOConVEX. J.P.V. thanks the Defense University Center at the Spanish Naval Academy (CUD-ENM) for all the support provided for this research. Funding for open access charge: Universidade de Vigo/CISUG.

References

[1] S.S. Sonawane, V. Juwar, Optimization of conditions for an enhancement of thermal conductivity and minimization of viscosity of ethylene glycol based Fe_3O_4 nanofluid, Appl. Therm. Eng. 109 (2016) 121.
[2] C.L. Altan, A. Elkatmis, M. Yüksel, N. Aslan, S. Bucak, Enhancement of thermal conductivity upon application of magnetic field to Fe_3O_4 nanofluids, J. Appl. Phys. 110 (2011) 093917.
[3] R. Fu, Z. Liu, Y. Chen, Y. Yan, Experimental investigation of turbulent forced heat transfer of Fe_3O_4 ethylene glycol–Water nanofluid with highly disaggregated particles, Therm. Sci. Eng. Prog. 10 (2019) 1.
[4] S. Rashidi, M. Eskandarian, O. Mahian, S. Poncet, Combination of nanofluid and inserts for heat transfer enhancement, J. Therm. Anal. Calorim. 135 (2019) 437.
[5] M. Izadi, A. Behzadmehr, M. Shahmardan, Effects of inclination angle on mixed convection heat transfer of a nanofluid in a square cavity, Int. J. Comput. Meth. Eng. Sci. Mech. 16 (2015) 11.
[6] M. Hatami, S. Mohammadi-Rezaei, M. Tahari, D. Jing, Recent developments in magneto-hydrodynamic Fe_3O_4 nanofluids for different molecular applications: a review study, J. Mol. Liq. 250 (2018) 244–258.
[7] A. Shahsavar, A. Godini, P.T. Sardari, D. Toghraie, H. Salehipour, Impact of variable fluid properties on forced convection of Fe_3O_4/CNT/water hybrid nanofluid in a double-pipe mini-channel heat exchanger, J. Therm. Anal. Calorim. 137 (2019) 1031.
[8] L.S. Sundar, M.K. Singh, A.C. Sousa, Thermal conductivity of ethylene glycol and water mixture based Fe_3O_4 nanofluid, Int. Commun. Heat Mass 49 (2013) 17.
[9] L. Syam Sundar, M.K. Singh, A.C.M. Sousa, Investigation of thermal conductivity and viscosity of Fe_3O_4 nanofluid for heat transfer applications, Int. Commun. Heat Mass 44 (2013) 7–14.
[10] N. Usri, W. Azmi, R. Mamat, K.A. Hamid, G. Najafi, Thermal conductivity enhancement of Al_2O_3 nanofluid in ethylene glycol and water mixture, Energy Proc. 79 (2015) 397.
[11] M. Abareshi, E.K. Goharshadi, S.M. Zebarjad, H.K. Fadafan, A. Youssefi, Fabrication, characterization and measurement of thermal conductivity of Fe_3O_4 nanofluids, J. Magn. Magn. Mater. 322 (2010) 3895.
[12] H. Xie, M. Fujii, X. Zhang, Effect of interfacial nanolayer on the effective thermal conductivity of nanoparticle-fluid mixture, Int. J. Heat Mass Transf. 48 (2005) 2926.
[13] J.A. Eastman, U. Choi, S. Li, L. Thompson, S. Lee, Argonne National Lab., IL (United States), 1996.
[14] H. Xie, J. Wang, T. Xi, Y. Liu, F. Ai, Q. Wu, Thermal conductivity enhancement of suspensions containing nanosized alumina particles, J. Appl. Phys. 91 (2002) 4568.
[15] S. Choi, Z. Zhang, W. Yu, F. Lockwood, E. Grulke, Anomalous thermal conductivity enhancement in nanotube suspensions, Appl. Phys. Lett. 79 (2001) 2252.
[16] T.-K. Hong, H.-S. Yang, C. Choi, Study of the enhanced thermal conductivity of Fe nanofluids, J. Appl. Phys. 97 (2005) 064311.
[17] K. Parekh, H.S. Lee, Magnetic field induced enhancement in thermal conductivity of magnetite nanofluid, J. Appl. Phys. 107 (2010) 09A310.
[18] W. Yu, H. Xie, L. Chen, Y. Li, Enhancement of thermal conductivity of kerosene-based Fe_3O_4 nanofluids prepared via phase-transfer method, Colloid Surf. A Physicochem. Eng. Asp. 355 (2010) 109.
[19] M. Afrand, D. Toghraie, N. Sina, Experimental study on thermal conductivity of water-based Fe_3O_4 nanofluid: development of a new correlation and modeled by artificial neural network, Int. Commun. Heat Mass 75 (2016) 262.
[20] M.-S. Izadkhah, H. Erfan-Niya, H. Moradkhani, Rheological Behavior of Water-Ethylene Glycol Based Graphene Oxide Nanofluids, Iran, J. Chem. Chem. Eng. 37 (2018) 177.
[21] R.S. Kumar, T. Sharma, Stability and rheological properties of nanofluids stabilized by SiO_2 nanoparticles and SiO_2-TiO_2 nanocomposites for oilfield applications, Colloid Surf. A Physicochem. Eng. Asp. 539 (2018) 171.
[22] M.A. Ramos-Docampo, M. Testa-Anta, B. Rivas-Murias, V. Salgueiriño, Clusters of Magnetite-Maghemite Nanocrystals with a Chemically-Tailored Average Diameter, J. Nanosci. Nanotechnol. 19 (2019) 4930.
[23] D7896-19, Standard test method for thermal conductivity, thermal diffusivity, and volumetric heat capacity of engine coolants and related fluids by transient hot wire liquid thermal conductivitymethod, ASTM Int. 2019, www.astm.org.
[24] A. Banisharif, M. Aghajani, S. Van Vaerenbergh, P. Estellé, A. Rashidi, Thermophysical properties of water ethylene glycol (WEG) mixture-based Fe_3O_4 nanofluids at low concentration and temperature, J. Mol. Liq. 302 (2020) 112606.
[25] S. Zeroual, P. Estellé, D. Cabaleiro, B. Vigolo, M. Emo, W. Halim, S. Ouaskit, Ethylene glycol based silver nanoparticles synthesized by polyol process: Characterization and thermophysical profile, J. Mol. Liq. 310 (2020) 113229.
[26] J. Sobczak, J.P. Vallejo, J. Traciak, S. Hamze, J. Fal, P. Estellé, L. Lugo, G. Żyła, Thermophysical profile of ethylene glycol based nanofluids containing two types of carbon black nanoparticles with different specific surface areas, J. Mol. Liq. 326 (2021) 115255.
[27] R. Otero-Lorenzo, M.A. Ramos-Docampo, B. Rodriguez-Gonzalez, M. Comesaña-Hermo, V.n. Salgueiriño, Solvothermal clustering of magnetic spinel ferrite nanocrystals: a Raman perspective, Chem. Mater. 29 (2017) 8729.
[28] J. Scott, Soft-mode spectroscopy: Experimental studies of structural phase transitions, Rev. Mod. Phys. 46 (1974) 83.
[29] B. Rivas-Murias, M. Testa-Anta, P. Torruella, S. Estradé, F. Peiró, B. Rodríguez-González, M. Comesaña-Hermo, V.n. Salgueiriño, Structural and Magnetic Implications of Transition Metal Migration within Octahedral Core-Shell Nanocrystals, Chem. Mater. 32 (2020) 10435.
[30] D.L. De Faria, S. Venâncio Silva, M. De Oliveira, Raman microspectroscopy of some iron oxides and oxyhydroxides, J. Raman Spectrosc. 28 (1997) 873.
[31] A.M. Jubb, H.C. Allen, Vibrational spectroscopic characterization of hematite, maghemite, and magnetite thin films produced by vapor deposition, ACS Appl. Mater. Interfaces 2 (2010) 2804.
[32] Babita, S.K. Sharma, S.M. Gupta, Preparation and evaluation of stable nanofluids for heat transfer application: a review, Exp. Therm. Fluid Sci. 79 (2016) 202–212.
[33] A. Ghadimi, R. Saidur, H. Metselaar, A review of nanofluid stability properties and characterization in stationary conditions, Int. J. Heat Mass Transf. 54 (2011) 4051.
[34] J.P. Vallejo, L. Mercatelli, M.R. Martina, D. Di Rosa, A. Dell'Oro, L. Lugo, E. Sani, Comparative study of different functionalized graphene-nanoplatelet aqueous nanofluids for solar energy applications, Renewable Energy 141 (2019) 791.
[35] M.P. Beck, Y. Yuan, P. Warrier, A.S. Teja, The effect of particle size on the thermal conductivity of alumina nanofluids, J. Nanoparticle Res. 11 (2009) 1129.
[36] G.-J. Lee, C.K. Rhee, Enhanced thermal conductivity of nanofluids containing graphene nanoplatelets prepared by ultrasound irradiation, J. Mater. Sci. 49 (2014) 1506.
[37] M. Mehrali, E. Sadeghinezhad, S.T. Latibari, S.N. Kazi, M. Mehrali, M.N.B.M. Zubir, H.S.C. Metselaar, Investigation of thermal conductivity and rheological properties of nanofluids containing graphene nanoplatelets, Nanoscale Res. Lett. 9 (2014) 1.
[38] M. Mehrali, E. Sadeghinezhad, M.A. Rosen, S.T. Latibari, M. Mehrali, H.S.C. Metselaar, S.N. Kazi, Effect of specific surface area on convective heat transfer of graphene nanoplatelet aqueous nanofluids, Exp. Therm. Fluid Sci. 68 (2015) 100.
[39] P.D. Shima, J. Philip, B. Raj, Synthesis of Aqueous and Nonaqueous Iron Oxide Nanofluids and Study of Temperature Dependence on Thermal Conductivity and Viscosity, J. Phys. Chem. C 114 (2010) 18825.
[40] J.P. Vallejo, J. Pérez-Tavernier, D. Cabaleiro, J. Fernández-Seara, L. Lugo, Potential heat transfer enhancement of functionalized graphene nanoplatelet dispersions in a propylene glycol-water mixture. Thermophysical profile, J. Chem. Thermodyn. 123 (2018) 174.
[41] M. Hadadian, E.K. Goharshadi, A. Youssefi, Electrical conductivity, thermal conductivity, and rheological properties of graphene oxide-based nanofluids, J. Nanoparticle Res. 16 (2014) 1.
[42] R. Agromayor, D. Cabaleiro, A.A. Pardinas, J.P. Vallejo, J. Fernandez-Seara, L. Lugo, Heat transfer performance of functionalized graphene nanoplatelet aqueous nanofluids, Materials 9 (2016) 455.
[43] H. Jiang, Q. Zhang, L. Shi, Effective thermal conductivity of carbon nanotube-based nanofluid, J. Taiwan Inst. Chem. Eng. 55 (2015) 76.
[44] X.-Q. Wang, A.S. Mujumdar, A review on nanofluids-part I: theoretical and numerical investigations, Braz. J. Chem. Eng. 25 (4) (2008) 613–630.
[45] J. Mølgaard, W. Smeltzer, Thermal conductivity of magnetite and hematite, J. Appl. Phys. 42 (1971) 3644.
[46] Y. Grosu, A. Faik, I. Ortega-Fernández, B. D'Aguanno, Natural Magnetite for thermal energy storage: Excellent thermophysical properties, reversible latent heat transition and controlled thermal conductivity, Sol. Energy Mater. Sol. Cells 161 (2017) 170.
[47] J. Rudl, C. Hanzelmann, S. Feja, A. Meyer, A. Potthoff, M.H. Buschmann, Laminar Pipe Flow with Mixed Convection under the Influence of Magnetic Field, Nanomaterials 11 (2021) 824.
[48] M.P. Spencer, W. Lee, A. Alsaati, C.M. Breznak, R. Braga Nogueira Branco, J. Dai, E.D. Gomez, A. Marconnet, P. von Lockette, N. Yamamoto, Cold sintering to form bulk maghemite for characterization beyond magnetic properties, Int. J. Ceram. Eng. Sci. 1 (2019) 119.
[49] J. Vallejo, E. Álvarez-Regueiro, D. Cabaleiro, J. Fernández-Seara, J. Fernández, L. Lugo, Functionalized graphene nanoplatelet nanofluids based on a commercial industrial antifreeze for the thermal performance enhancement of wind turbines, Appl. Therm. Eng. 152 (2019) 113.

[50] M.M. Tawfik, Experimental studies of nanofluid thermal conductivity enhancement and applications: A review, Renew. Sustain. Energy Rev. 75 (2017) 1239–1253.
[51] H.Ş. Aybar, M. Sharifpur, M.R. Azizian, M. Mehrabi, J.P. Meyer, A review of thermal conductivity models for nanofluids, Heat Transf. Eng. 36 (2015) 1085.
[52] Y. Ding, H. Alias, D. Wen, R.A. Williams, Heat transfer of aqueous suspensions of carbon nanotubes (CNT nanofluids), Int. J. Heat Mass Transf. 49 (2006) 240.
[53] S.A. Putnam, D.G. Cahill, P.V. Braun, Z. Ge, R.G. Shimmin, Thermal conductivity of nanoparticle suspensions, J. Appl. Phys. 99 (2006) 084308.
[54] A. Ceylan, K. Jastrzembski, S.I. Shah, Enhanced solubility Ag-Cu nanoparticles and their thermal transport properties, Metall. Mater. Trans. A 37 (2006) 2033.